The role of the stress-path and importance of stress history on the flow of water along fractures and faults; an experimental study conducted on kaolinite gouge and Callovo-Oxfordian mudstone

Robert J. Cuss, Jon F. Harrington, British Geological Survey, Keyworth, Nottingham, NG12 5GG, UK

Shanvas Sathar, Present address: Alberta Energy Regulator (AER), Centennial Place, 250 5th Street SW, Calgary - T2P 0R4, Alberta, Canada

Simon Norris, Radioactive Waste Management Limited, Building 587, Curie Avenue, Harwell Science and Innovation Campus, Didcot, Oxfordshire, OX11 0RH, UK

Jean Talandier, Andra, 1-7, rue Jean Monnet, 92298 Chatenay-Malabry, France

Corresponding author: R.J. Cuss, British Geological Survey, Keyworth, Nottingham, NG12 5GG, UK. (rjcu@bgs.ac.uk)

Key points:

- Importance of stress history on fracture flow.

- Stress dependency of fracture flow described by a power-law or cubic relationship.

- Fracture flow dependent on fracture roughness, thickness of gouge material, saturation state, permeability of the host material, clay mineralogy, and the degree of shearing.

19 ***Abstract:*** *The flow of water along discontinuities, such as fractures or faults, is of paramount*

20 *importance in understanding the hydromechanical response of an underground geological*

21 *disposal facility for radioactive waste. This paper reports four experiments conducted on*

22 *kaolinite gouge on a 30° slip-plane and on realistic fractures created in Callovo-Oxfordian*

23 *mudstone (COx) from France. Test histories were conducted that initially loaded the gouge*

24 *material in step changes in vertical stress, followed by unloading of the sample in similar*

25 *steps. This loading-unloading history showed considerable hysteresis in hydraulic flow, with*

26 *only partial recovery of fracture transmissivity. This demonstrates the importance of stress*

27 *history on fracture flow; consideration of just the current stress acting upon a fracture or*

28 *fault may result in inaccuracies of predicted hydraulic flow. The stress dependency of*

29 *fracture flow in both kaolinite and COx can be described by a power-law or cubic*

30 *relationship, which is likely to be dependent on the fracture roughness, thickness of gouge*

31 *material, saturation state, permeability of the host material, and clay mineralogy (i.e.*

32 *swelling potential). The observed response of fracture transmissivity to normal stress in COx*

33 *is a complex superposition of mechanical response of the fracture and the swelling of clay*

34 *in the fracture surface. The stress-dependency of flow was also seen to be dependent on*

35 *orientation with respect to bedding. A fracture perpendicular with bedding accommodates*

36 *greater compression and results in a lower transmissivity. The orientation dependence is*

37 *related to the anisotropic swelling characteristics of COx.*

38 **Keywords**

1. Introduction

Discontinuities (fracture, faults, joints, interfaces, etc.) play a key role in controlling the movement of water and gas around an underground Geological Disposal Facility (GDF) for radioactive waste. High Level Waste (HLW), Intermediate Level Waste (ILW) and some long-lived low-level radioactive waste and spent fuel are planned to be disposed of in a GDF within stable geological formations at depth (~200-800 m) by a number of countries. The disposal concept incorporates waste isolation and containment by engineered and geological barriers in such a facility. At depth the rock mass may be a naturally fractured environment, as in the case for crystalline rocks. The stress re-distribution resulting from the excavation of tunnels in both crystalline and clay-rich host rocks will result in the formation of the Engineered Disturbed Zone (EDZ), where an intricate range of discontinuity orientations are present in a complex localized stress field (Bossart *et al.*, 2002, 2004; Rutqvist *et al.*, 2009, Armand *et al.*, 2014). Therefore, most current disposal concepts will include a multitude of discontinuities as part of the natural and engineered environment, which will be present for varying time-scales dependent on the host-rock; i.e. the EDZ is likely to self-seal in a clay-rich formation, whereas it will persist for extended periods in a crystalline rock type. Depending on the *in situ* stress conditions and whether self-sealing has resulted in fracture closure, preferential pathways for fluid movement may form along any, all, or none of these discontinuities.

There are a number of potential events that may change the stress state that acts upon any fractures present in a GDF host rock. The modelling work of Barla and co-workers (Barla, 1999; Bonini *et al.*, 2001) showed that during the excavation of a tunnel the stress field is altered and the surrounding rock-mass follows a stress path. This results in changes in stress acting on existing discontinuities and, following their formation, a change in the stress acting on EDZ fractures. The process of closing a GDF is likely to be achieved by backfilling open spaces (access tunnels, etc.) with bentonite/sand mixtures or crushed host rock material

66   (depending on disposal concept). This will result in swelling of clay-based materials on

67   resaturation and the transmission of stress to the EDZ, resulting in a further change to the stress

68   experienced by any discontinuities present in the host rock. Over geological timescales in

69   certain parts of northern and northwestern Europe, there may be increased stress on the GDF

70   as the result of glacial loading, or a reduction in stress as the result of erosion of some of the

71   over-burden, although this is unlikely in France. Therefore, over the full history of the GDF

72   several scenarios may occur that could result in changes in the stress acting upon discontinuities

73   of varying time-scales.

74   The evolution of permeability in rocks under hydrostatic stress conditions has been widely

75   reported. The stress dependency of permeability has been reported under hydrostatic stress

76   conditions in a number of different rock types (e.g. Zoback & Byerlee 1975; Walsh & Brace

77   1984; Morrow *et al*., 1984; Neuzil *et al*., 1984; David *et al*., 1994; Dewhurst *et al*., 1999[1,2];

78   Katsube, 2000; Katsube *et al*., 1996[1,2]; Kwon *et al*., 2001; Zhang & Rothfuchs, 2004).

79   However, in the field, rocks are subject to an inhomogeneous stress-field, where the vertical

80   stress (determined by the weight of the overburden) exceeds the orthogonal maximum and

81   minimum horizontal stresses (Holt, 1990). This has led to investigations of the sensitivity of

82   matrix permeability to non-hydrostatic stress conditions, especially in sandstones (e.g.; Zhu &

83   Wong, 1994; Zhu & Wong, 1997; Keaney *et al*., 1998). The reported permeability for intact

84   shale, mudstones, and clay-rich rocks subjected to hydrostatic pressures varies from 10^{-16} m^2

85   to 10^{-23} m^2 (Kwon *et al*., 2001). Many researchers have shown that the permeability of shale

86   decreases with externally applied stress (Neuzil *et al*., 1984; Katsube *et al*., 1996[1,2]; Dewhurst

87   *et al*., 1999[1,2]; Katsube, 2000; Kwon *et al*., 2001;) and decreased porosity (Schloemer & Kloss,

88   1997; Dewhurst *et al*., 1998). A number of non-linear relationships have been proposed

89   between permeability, porosity, and pressure in shale and mudstones, including exponential

90　　and power laws between permeability and pressure (Katsube *et al*., 1991; Dewhurst *et al*.,

91　　1999[1]).

92　　The permeability, or transmissivity, of discontinuities and its associated relationship with stress

93　　has not been widely reported. The Compression of the Damaged Zone (CDZ) experiment

94　　conducted at the Meuse/Haute-Marne Underground Research Laboratory (URL) at Bure,

95　　approximately 300 km east of Paris, demonstrated that the transmissivity of fractures formed

96　　around the EDZ was sensitive to the loading experienced (de La Vaissière *et al*., 2015). Only

97　　a small effect was seen in the transmissivity to gas, but clay/water interactions led to a decrease

98　　of water permeability of several orders of magnitude. In Opalinus Clay (OPA), the load plate

99　　experiment at the Mont Terri URL observed a fracture transmissivity decrease with increasing

100　　load pressures by up to a factor of 60 (Bühler *et al*., 2003). Careful experimental design proved

101　　that the decrease in transmissivity follows the stepwise increase of the load pressure and was

102　　due to mechanical compression of the fracture network. A longer-term reduction in

103　　transmissivity was also observed, which may be related to swelling and rearrangement of clay

104　　minerals. In the load plate experiment the transmissivity seen at the highest load was still

105　　greater than that for intact OPA. However, at the Meuse/Haute-Marne URL, permeability has

106　　been observed to return to that of the intact material within the uncertainty of water

107　　permeability for COx. Several laboratory experimental studies have been conducted examining

108　　fracture flow in Callovo-Oxfordian mudstone, including Davy *et al.* (2007), Foct *et al.* (2012),

109　　Zhang *et al.* (2013), and Auvray *et al.* (2015).

110　　Gutierrez *et al*. (2000) experimentally investigated the hydromechanical behaviour of an

111　　extensional fracture in Kimmeridge Shale under normal and shear loading. At the time the

112　　fracture was created it had a higher permeability than the equivalent permeability of the intact

113　　shale. Increasing the contact normal stress across the fracture reduced the fracture permeability

114　　following an empirical exponential law. However, loading the sample to an effective normal

115   stress twice as much as the intact rock unconfined compressive strength did not completely

116   close the fracture, although it did reduce the permeability by an order of magnitude. Cuss *et al.*

117   (2011) showed that fracture transmissivity in OPA decreased linearly with an increase in

118   normal load over a limited stress range. This study also showed that shear movement along the

119   fracture resulted in effective self-sealing in OPA and reduced hydraulic fracture transmissivity

120   to similar levels to that of the intact material. A one order of magnitude reduction in fracture

121   transmissivity of OPA just in response to re-hydration of the fracture because of the swelling

122   of the clay minerals has been reported (Cuss *et al.,* 2014; Cuss & Harrington, 2014). A further

123   order of magnitude reduction was observed in response to shearing along the fracture, this may

124   be in part due to clay smearing and mineral rearrangement and/or due to a greater number of

125   clay minerals coming into contact with water and swelling as a result of the formation of

126   microfractures sub-parallel to the main fracture.

127   The objective of the current experimental program was to investigate the water flow properties

128   of a discontinuity at 30° to changes in vertical load and to compare these observations with the

129   recorded flow in a horizontal fracture formed in Callovo-Oxfordian mudstone (COx). This

130   would simulate effective stress changes, such as pore-pressure variations on faults or stress

131   changes associated with GDF closure. As stated above, the response of fracture flow to changes

132   in normal stress are dependent on the rock-type that the fracture exists. Previous experimental

133   work at the British Geological Survey (BGS) on fracture transmissivity in Opalinus Clay (Cuss

134   *et al.*, 2011; 2014; Cuss & Harrington, 2014) showed that hydraulic flow is a complex, focused,

135   transient property that is dependent upon normal stress, shear displacement, fracture topology,

136   fluid composition, and clay swelling characteristics. The current experimental program aimed

137   to extend this knowledge by investigating the influence of vertical stress on water flow through

138   gouge-filled discontinuities and in COx. The response of discontinuities has two clear

139   components; a mechanical response to load and a response from swelling effects of clay

140   minerals. Comparing results from two experimental geometries would allow mechanical and

141   swelling effects to be determined. The observations from the 30°discontinuity also are relevant

142   to non-swelling fractures, such as those seen in crystalline environments.

2. Experimental setup

144   Experiments were performed using two similar bespoke shear apparatus, designed and built at

145   BGS. The Direct Shear Rig (DSR, Figure 1a) was designed to study fracture transmissivity in

146   clay-rich rock samples. The Angled Shear Rig (ASR, Figure 1b) was designed to study fault

147   flow in a generic synthetic fault gouge at varying angles to the stress field.

148   Both the DSR and ASR are comprised of six key components:

149   1. Rigid steel frame that had been designed to deform as little as possible during the
150   experiment;

151   2. Vertical load system comprising an Enerpac hydraulic ram that was controlled using a
152   Teledyne/ISCO 260D syringe pump, a rigid loading frame and an upper thrust block (up to
153   20 MPa normal stress, 72 kN force). The Enerpac ram had a maximum stroke of 105 mm,
154   which meant that it could easily accommodate the vertical displacement of the top block of
155   the ASR as it rode up the fault surface at constant vertical load. Vertical travel of the thrust
156   block was measured by a high precision non-contact capacitance displacement transducer,
157   which had a full range of ± 0.5 mm and an accuracy of 0.06 µm;

158   3. Shear force actuator comprised of a modified and horizontally mounted Teledyne/ISCO
159   500D syringe pump designed to drive shear as slow as 14 microns a day at a constant rate
160   (equivalent to 1 mm in 69 days) or as fast as 0.5 mm per second along a low friction bearing.
161   The movement of the bottom-block was measured using a linear variable differential
162   transformer (LVDT), which had a full range of ± 25 mm and an accuracy of 0.5 µm;

163   4. Pore pressure system comprising a Teledyne/ISCO 500D syringe pump that could deliver

164   either water up to a pressure of 25.8 MPa. The syringe pump delivered water directly to the

165   fracture surface;

166   5. A state-of-the-art custom designed data acquisition system using National Instruments

167   LabVIEW™ software facilitating the remote monitoring and control of all experimental

168   parameters;

169   6. A sample assembly, which was the main difference between the DSR and ASR. In both

170   experimental setups, the bottom block was actively sheared and the top block was

171   connected through a linkage system to a force gauge measuring the shear stress along the

172   slip plane.

173   a. DSR: two samples of 60 mm × 60 mm × ~25 mm were held by two stainless steel

174   holders. Vertical load was applied to the rock samples by means of a steel thrust block.

175   A 4 mm bore the same length as the upper fractured block delivered pore fluid through

176   the top sample directly to the fracture surface.

177   b. ASR: the sample assembly consisted of polished precision-machined 316 stainless steel

178   top and bottom blocks (thrust blocks) with a dip of 30 degrees with respect to horizontal.

179   Fluid was introduced through a 4 mm filter in the centre of the top block. Two additional

180   4 mm diameter filters positioned orthogonally to each other at 15 mm from the central

181   pore fluid inlet were connected to pore-pressure transducers in order to monitor pressure

182   within the gouge (see Figure 1b). The lower thrust block was longer than the 60 mm ×

183   60 mm upper thrust block in order to maintain a constant contact area during shearing.

184   Two high precision eddy current non-contact displacement transducers were located

185   either end of the top thrust block and recorded gouge thickness directly and determined

186   non-parallel alignment of the two thrust blocks. These submersible devices had a full

187   range of ± 1 mm and an accuracy of 0.2 µm.

2.1 Test material and experimental protocols

189   For the tests conducted using the DSR, a sample of Callovo-Oxfordian mudstone[1] (COx) was

190   used from material extracted from the Meuse/Haute-Marne underground research laboratory at

191   Bure in France. Yven *et al.* (2007) report three main mineral phases; clay minerals, quartz and

192   calcite. Secondary mineral phases include dolomite, feldspar, pyrite, hematite and traces of

193   siderite. Calcite and quartz represent $40 - 55\%$ of the rock. Clay represents $20 - 55\%$, with

194   secondary minerals forming less than 5%. Clay minerals include illite and illite-smectite with

195   subordinate kaolinite and chlorite. Upon receipt of the preserved core barrels at BGS, the

196   material was catalogued and stored under refrigerated conditions of 4°C to minimize biological

197   and chemical degradation. The preserved core barrels consisted of a multi-layered arrangement

198   designed to re-stress the core to *in situ* stress and to environmentally seal it in order to reduce

199   chemical, biological and drying effects. Both test samples were prepared from core material

200   from borehole OHZ1607, which was drilled horizontal to bedding with a diameter of 100 mm.

201   Table 1 summarizes the origin of the core material and the properties of the test samples. The

202   test samples were prepared by dry cutting an approximate $60 \times 60 \times 50$ mm block from core

203   barrel material. The faces were ground flat and parallel using a diamond mill so as produce a

204   good fit into the sample holders. The starting water saturation is reported in Table 2, along with

205   the geotechnical properties of the starting material. The samples were wrapped in cling-film

206   and between test stages were stored in two sealed bags to reduce the possibility of drying.

---

[1] The Callovo-Oxfordian mudstone (COx) from the Meuse/Haute-Marne URL is often referred to as the Callovo-Oxfordian claystone. However, it does not always consist of clay minerals greater than 50 % volume and as such is not necessarily a true claystone. Therefore, the term mudstone is used. Please note COx is also referred to as Callovo-Oxfordian claystone/argillite/formation/clay rock/mudstone/argillaceous rock/shale.

207   A fracture was created in the cubic sample by shearing in the DSR apparatus. As the sample

208   was rigidly held by two steel holders, the shearing action resulted in a realistic fracture being

209   formed at the junction between the two holders. This created two samples of approximately 25

210   mm thickness. A bore of 4 mm diameter was drilled in the top fracture sample in order to

211   accommodate the pore injection pipe of the upper thrust block. During fluid injection a

212   chemically balanced synthetic pore fluid was used similar to that found at Bure (Gaucher *et al.*,

213   2007). This was manufactured at BGS with the following composition: 227 mg l^{-1} Ca^{2+}, 125

214   mg l^{-1} Mg^{2+}, 1012 mg l^{-1} Na^{+}, 35.7 mg l^{-1} K^{+}, 1240 mg l^{-1} Cl^{-}, 1266 mg l^{-1} SO_4^{2-}, 4.59 mg l^{-1}

215   Si, 9.83 mg l^{-1} SiO_2, 13.5 mg l^{-1} Sr, 423 mg l^{-1} total S, and 0.941 mg l^{-1} total Fe.

216   Following fracture creation, the two fracture surfaces were scanned using a NextEngine 3D

217   Scanner HD. This produces a 3D mesh model of the fracture surface accurate within an error

218   of ± 65 microns. Algorithms inbuilt within the data acquisition ScanStudio HD software

219   produced clean surface data which were used in subsequent empirical and statistical analysis.

220   Fracture roughness and other standard measurements were made using TrueMap 5.0 surface

221   topography software. A small quantity of disaggregated clay may have been lost during the

222   scanning process, although this was minimal, with only a few milligrams of clay dislodged

223   from the fracture surface. The fracture surfaces were exposed to air for a maximum of five

224   minutes during scanning and were placed in sealed sample bags at all other times. This was to

225   reduce moisture loss, which over this short period of time is assumed to be negligible.

226   For tests conducted using the ASR, a gouge material for the experiments was prepared from

227   powdered kaolinite (Supreme Powder); 16 ± 0.1 g of de-ionized water was added to 20 ± 0.1 g

228   of kaolinite powder. The water and kaolinite were then stirred for five minutes giving a

229   kaolinite paste with a gravimetric water content of 80 ± 1%, or a saturation state close to 100%

230   (see Table 2). The paste was smeared uniformly onto the surface of the top block, which was

231   then carefully lowered onto the bottom block thus forming a kaolinite paste gouge. The initial

232 thickness of the gouge was determined to be of the order of one millimetre. However, as no

233 lateral confinement was made of the clay gouge, thickness decreased to approximately 70 ± 10

234 µm with loading and clay was squeezed from between the thrust blocks. The apparatus was

235 designed without lateral gouge confinement as this would require sealing elements that would

236 have a high frictional component along the fault surface compared with the low frictional

237 properties of kaolinite. Initial loading resulted in excess clay being squeezed out from the fault

238 surface; this excess material prevented water from the shear bath entering the fault gouge or

239 from causing sloughing.

240 In the ASR, a constant pore pressure of approximately 1 MPa was created carefully once a

241 small vertical stress had been imposed on the fracture surface. Care was taken to ensure that

242 kaolinite was not eroded from the slip plane by limiting flowrate to sub-100 µl h^{-1}. At low

243 normal stresses, the fractures in COx could not be limited to 100 µl h^{-1} at such a high pore-

244 pressure. For test DSR_COx_01, pore pressure was slowly increased in steps from 120 kPa to

245 500 kPa during the hydration stage, with 750 kPa used during the flow test. At all steps flow

246 was kept below sub-500 µl h^{-1}. For test DSR_COx_02 an initial flow rate of 100 µl h^{-1} was

247 imposed until a pore pressure of 150 kPa was achieved, all further testing was then undertaken

248 at a constant pore pressure of 150 kPa. All measures were taken to limit erosion of clay from

249 the fracture surfaces in all tests. Once stable flow had been achieved, the vertical stress was

250 increased (or decreased) in regular steps. The flow rate of the injection system was monitored

251 and used to determine fracture transmissivity.

252 **2.2 Data reduction**

253 Fracture transmissivity was calculated assuming radial flow from the injection hole given the

254 steady state fluid flow rate Q and the pressure head H at the injection point. Steady flow in a

255 cylindrical geometry is given by:

256
$$Q = \frac{2\pi T\left(h_i - h_0\right)}{\ln\left(r_o\right) - \ln\left(r_i\right)}$$
[1]

257   where T is the transmissivity, h_i is the head on the inner surface with radius r_i, and h_o is the

258   head on the outer surface at radius r_o (Gutierrez *et al.*, 2000). For the experimental setup r_0 =

259   30 mm, r_i = 1.96 mm, h_0 = 0.05 m and $h_i \sim$ 100 m. Substituting these constants into equation 1

260   gives transmissivity ($m^2\ s^{-1}$):

261
$$T = 1.183 \times 10^{-12}\, \frac{Q}{P_p}$$
[2]

262   if the fluid flux (Q in $\mu l\ h^{-1}$) and pore pressure (P_p in kPa) are known. This relationship was

263   used to calculate the transmissivity of the fracture throughout the experiment. It should be noted

264   that Equation 1 relates to a circular sample, whereas the fracture is created in a cubic sample.

265   Therefore, it is assumed that the shortest distance between the injection point and the edge of

266   the sample is the controlling factor. It should also be noted that as the fracture is sheared the

267   contact area between the top and bottom face of the fracture reduces. As a result, the shortest

268   distance to the edge of the sample (r_o) effectively reduces. Scoping calculations showed this

269   had a negligible effect on the overall calculation.

270   **3.0 Experimental results for Angled Shear Rig (Kaolinite gouge)**

271   Two load-unload experiments were conducted using the ASR apparatus with water as the

272   injection fluid, both on a 30° slip-plane (Table 2). Figure 2 shows an example of the data

273   recorded during hydraulic flow for test ASR_Tau05_30wLU plotted against time, whereas data

274   plotted against vertical stress are shown in Figure 3. Vertical stress was sequentially increased

275   in stages of 0.2 MPa per day from an initial 0.2 MPa to a maximum vertical stress of 2.6 MPa

276   (Figure 2b). The pore fluid injection pressure was maintained at a constant value of 1 MPa.

277   Although no horizontal stress was applied, the increase in horizontal stress as a consequence

278   of vertical stress increase was logged throughout the duration of the experiment. During the

279   unloading stage, the vertical stress was decreased in steps of 0.2 MPa from 2.6 MPa to 0.2

280   MPa. Temperature remained uniform at 20.5 ± 0.1°C throughout the entire duration of the

281   experiment (Figure 2a). The flow rate decreased an order of magnitude from 50 µl h^{-1} to 5 µl

282   h^{-1} during loading from 0 to 2.6 MPa. During unloading from 2.6 to 0.2 MPa, flow rate doubled

283   from 5 µl h^{-1} to 10 µl h^{-1}. From 2.6 MPa to 1.0 MPa vertical stress, the flow rate remained

284   constant at 5 µl.h^{-1} irrespective of the significant reduction in vertical load (Figure 2c, Figure

285   3a). Pore pressure within the slip plane recorded much lower pressures (50 – 80 kPa and 5 –

286   25 kPa) than the injection pressure (1 MPa) (Figure 2d). During loading, fracture transmissivity

287   decreased from 5×10^{-14} m^2 s^{-1} to 0.6×10^{-14} m^2 s^{-1}. However, during unloading transmissivity

288   recovered to only 1.1×10^{-14} m^2 s^{-1}. The thickness of the kaolinite gouge decreased with loading

289   from 54 µm at a vertical stress of 0.2 MPa to 42 µm at a vertical stress of 2.6 MPa. During

290   unloading, the slip plane width continued to decrease further to 40 µm before finally recovering

291   to 43 µm after full unloading (Figure 2e, Figure 3b). Vertical displacement was seen to reduce

292   by nearly 350 µm during the loading stage, with a hysteretic recovery during unload (Figure

293   2f, Figure 3c). No significant differences were seen between tests ASR_Tau05_30wLU and

294   test ASR_Tau01_30wLU, as shown in Cuss *et al.* (2013).

295   Figure 4 shows the results of flow achieved for the two tests conducted injecting water into a

296   30° discontinuity during loading from 0.1 to 2.6 MPa and unloading from 2.6 to 0.2 MPa. As

297   can be seen, the starting flow rates of the two tests were different by nearly a factor of 2. Both

298   tests were setup in identical ways using the same pre-mixed weight of kaolinite and deionised

299   water. The difference is likely to be related to differences in gouge thickness. As normal load

300   was increased in steps, the flow along the slip plane steadily reduced. In both experiments,

301   although starting from dissimilar flow rates, a flow rate of approximately 6 µl h^{-1} at a vertical

302   stress of 2.6 MPa was achieved. As both experiments resulted in a similar flow, it is suggested

303 that the final gouge thickness was similar for both tests following expulsion of excess clay

304 during loading. The difference may also be due to variation in starting saturation of the kaolinite

305 gouge, although every care was taken to produce gouge material that was identical. As reported

306 in Cuss *et al.* (2013), shear is seen to be an effective self-sealing mechanism in kaolinite gouge,

307 significantly reducing flow. Therefore, differences in starting transmissivity may also be

308 related to the degree of shearing experienced during the setting up of the experiment. On

309 unloading, this flow rate did not significantly alter until a vertical load of approximately 0.75

310 MPa was reached.

311 **3.1 Experimental results for Direct Shear Rig (COx)**

312 Two experiments were conducted using the DSR on samples of COx, as described in Table 2.

313 The first test (DSR_COx_01) was a simple loading history in order to describe the stress

314 dependency of fracture transmissivity. The second test (DSR_COx_02) was a more detailed

315 load-unload-reload test history. It should be noted that the orientation of the two tests were

316 different, with test DSR_COx_01 fractured parallel to bedding, while DSR_COx_02 was

317 fractured perpendicular to bedding.

318 The results from the first test that was performed are shown in Figure 5. The test history is

319 shown as two separate tests due to the behaviour recorded. Previous testing conducted in

320 Opalinus Clay (e.g. Cuss *et al.*, 2011) showed that the injection of pore fluid or the change in

321 normal load resulted in a transient response in fracture transmissivity that would equilibrate

322 within a few days. As shown in Figure 5e, the initial test step showed a short transient, giving

323 an average flow rate of 99 μl h^{-1} at 2.07 MPa after 72 hours. Normal load was increased to 2.5

324 MPa and a considerable transient was observed. As clearly seen, a full asymptote of the flow

325 rate had not been achieved after 1,512 hours (2 months). As well as a continually changing

326 response for flow, a small component of normal displacement was seen that similarly had not

327 reached equilibrium (Figure 5g). It was not feasible to continue the experiment at such a slow

328 rate and the decision was taken to begin a new phase of experimentation with step changes in

329 normal load being conducted on 24-hour periods. This was deemed sufficient to allow the

330 transient associated with a change in normal load to equilibrate and to be a good representation

331 of the mechanical change in flow properties without the influence of long-term changes in flow

332 properties associated with clay swelling. This phase of experimentation is shown in Figure

333 5b,d,f,h. Results shown in Figure 5b are affected by the air conditioning in the laboratory,

334 which was not stable at the time these results were collected due to an intermittent fault (this

335 fault affected no other experiments). Overall, air conditioning issues did not have a detrimental

336 influence on flow in relation to results shown in Figure 5f, although a short-term variation is

337 seen. It was still possible to determine an average flow for each normal load step. During the

338 full duration of the experiment, flow reduced from 100 µl h^{-1} at 2.07 MPa to 40 µl h^{-1} at 3.85

339 MPa. Figure 8 shows that a good relationship was observed with a decreasing fracture

340 transmissivity from 1.6×10^{-13} m^2 s^{-1} to 4.2×10^{-14} m^2 s^{-1} as normal load increased from 2 to

341 3.85 MPa.

342 Figure 6 shows the data recorded during hydraulic flow test DSR_COx_02 during a load-

343 unload-reload (LUR) history plotted against time, data plotted against normal stress is shown

344 in Figure 7. Normal stress was sequentially increased in steps of 0.15 or 0.4 MPa from an initial

345 0.54 MPa to a maximum normal stress of 1.67 MPa (Figure 6b). Each step was conducted until

346 flow rate stabilized and ranged in duration from 1 to 24 hours. Due to high flow rates seen at

347 low normal stresses, the pore fluid injection pressure was maintained at constant values of

348 between 0.15 and 0.25 MPa, as shown in Figure 6b. During the unloading stage, the normal

349 stress was decreased in steps of 0.25 or 0.45 MPa from 1.67 MPa to 0.53 MPa. The reload

350 stage saw normal stress increased in steps of between 0.2 and 0.45 MPa from 0.53 MPa to a

351 new maximum normal stress of 3.42 MPa. Temperature remained uniform at 21.25 ± 0.1 °C

352 throughout the entire duration of the experiment (Figure 6a).

353 The early flow rate history was very complex (Figure 6c, Figure 7a). The observations stated

354 above for tests conducted on kaolinite gouge showed a distinct hysteresis during unloading;

355 therefore, it was vital that normal load was increased from a starting low normal stress. This

356 was complicated by issues related to erosion along the fracture surface and the necessity to

357 ensure that excessive flow rates were not sustained. This resulted in variations in pore injection

358 pressure and duration of stages. Post experiment examination of the sample did not highlight

359 any features of erosion on the fracture surface. The initial stage had a high flow rate of 1,600

360 $\mu l\ h^{-1}$ at 0.54 MPa, which reduced to 142 $\mu l\ h^{-1}$ at 1.67 MPa. During the unloading stage there

361 was a partial recovery of flow to 257 $\mu l\ h^{-1}$ as normal stress was reduced to 0.53 MPa. During

362 reloading to the previous maximum normal stress of 1.67 MPa the flow reduced to 120 $\mu l\ h^{-1}$,

363 which is similar to the flow rate that was recorded at the end of the initial loading phase. As

364 normal stress was increased to the new maximum of 3.42 MPa the flow rate reduced to 7.3 μl

365 h^{-1}. Therefore, during the duration of the experiment the fracture transmissivity reduced from

366 $1.3 \times 10^{-11}\ m^2\ s^{-1}$ to $5.7 \times 10^{-14}\ m^2\ s^{-1}$. Figure 6d and Figure 7b show the results for normal

367 displacement. As shown, a near linear reduction in normal displacement was observed during

368 loading, with a small degree of hysteresis seen on unloading. Only 0.25 mm of normal

369 displacement was seen during the full test history.

370 **4 Discussion**

371 The current study has utilized both kaolinite gouge as an analogue fracture and a shear fracture

372 created in COx. The use of a kaolinite gouge was in order to reduce the number of variables in

373 the experiments by effectively eliminating fracture roughness and the presence of asperities.

374 The selection of kaolinite was determined by the low swelling capacity of the clay, facilitating

375   quicker experiments and the study of a greater number of features of fracture flow. The limited

376   swelling capacity also means that the fluid flow behaviour is dominated by the mechanical

377   response of flow to loading. In contrast, COx has a high content of swelling clay (illite and

378   illite-smectite), which means that observations listed above are a combination of the

379   mechanical response of loading and the swelling response of the clay minerals on the fracture

380   surface. However, comparisons can still be made in the behaviour observed in both kaolinite

381   and COx fractures, with the kaolinite results aiding the separation of mechanical and swelling

382   responses in COx. Figure 8 shows that when viewed in log vertical stress versus log fracture

383   transmissivity space, linear regions of the data are clearly defined, signifying a power-law

384   relationship between stress and fracture transmissivity for all the current tests.

385   As seen in Figure 8, the only exception to the power-law behaviour is test DSR_COx_02,

386   although this discrepancy can be explained. As stated earlier, the initial test history was

387   dominated by the need to minimize flow through the fracture and to ensure that erosion of the

388   fracture surface did not occur. The created fracture would have had mismatch between the

389   fracture surfaces, resulting in asperities and a higher transmissivity than for a perfectly matched

390   fracture surface. As vertical stress was increased in the experiment, these asperities became

391   less dominant and flow reduced, and during this phase of the test history a linear relationship

392   can be used to describe the dependence of transmissivity on stress. During this period of the

393   test, swelling would also have been a dominant process and the necessity to keep test stages

394   short meant that full equilibration per stage had not been reached. However, at approximately

395   1.7 MPa vertical stress, the behaviour changed: at this stress level the asperities have closed

396   and the fracture began to show a power-law relationship between stress and flow. This

397   transition was not seen in test DSR_COx_01 for two reasons. Firstly, the minimum stress

398   exceeded 2 MPa, therefore asperities created by mismatch may have closed. Secondly, the first

399   stage of the test resulted in a prolonged period of rehydration and swelling on the fracture

400   surface may have caused the mismatch to have been sealed.

401   Close examination of test data for DSR_COx_02 suggests that a further change in behaviour

402   may have happened at around 2.75 MPa. This can be interpreted as a slip event on the fracture

403   surface. The increasing vertical stress has become sufficient that the mismatch has resulted in

404   a small movement along the fracture. Shear has been shown to be an effective self-sealing

405   mechanism in fracture experiments (e.g. Cuss *et al.*, 2011; 2013; 2014) and this would result

406   in a decrease in fracture transmissivity. Close examination of all recorded data is not conclusive

407   on whether movement occurred or not. However, a decline in shear stress around this time

408   suggests movement did occur. Therefore, the alternative power-law fit shown in Figure 8a and

409   Table 3 is more representative of the relationship between stress and flow. It has to be

410   acknowledged that true steady-state conditions were not achieved in all test stages and that as

411   well as the mechanical closure of the fracture there is an ongoing reduction in flow related to

412   self-sealing and swelling of clay minerals. These observations are in contradiction to the CDZ

413   field test (de La Vaissière *et al.*, 2015).

414   Berkowitz (2002) extensively reviewed flow though fractures and fractured rocks. Several

415   models of relationships of fracture flow with increasing normal stress exist, based on linear,

416   cubic, exponential and power-laws. During the current study, no appraisal has been made of

417   the validity of the available models. However, as shown in Figure 9 and Table 4, the data from

418   the current study have been fitted using a range of empirical relationships between flow and

419   vertical stress. In Table 4 the highlighted values represent the relationships that have the highest

420   value of R^2 and therefore are statistically the best fit to the data, although this approach does

421   not necessarily represent the best fit to the data in a physical sense. All relationships (power-

422   law, exponential, logarithmic and cubic) offer a good approximation of the data, although the

423   linear relationship is poor in most tests. It can be seen that a cubic relationship offers the best

424 fits to the loading data, although good fits are achieved with power-law, exponential and

425 logarithmic relationships. Both cubic and power-law relationships offer good descriptions of

426 the flow behaviour during unloading. Table 4 suggests that a cubic relationship best describes

427 the flow properties of fractures during loading and unloading.

428 Figure 9c shows data from the CDZ (Compression of the Damaged Zone) in situ experiment

429 conducted at the Meuse/Haute-Marne URL (de La Vaissière *et al.*, 2015). Data is shown for

430 boreholes CDZ1305 and CDZ1306, which were behind a hydraulic loading plate installed in

431 the GET drift. The hydraulic ram loaded the walls of the tunnel and resulted in the closure of

432 the damage zone around the tunnel. As shown, data for conductivity at different loading

433 stresses are also well described by a cubic law. These data are not well described by a power-

434 law relationship. Therefore, a cubic law describes the relationship between loading and flow

435 seen in Callovo-Oxfordian mudstone.

436 The current study has highlighted the significance of stress history with the non- or partial-

437 recovery of flow during unloading. In all tests that included unloading stages, irrespective of

438 whether gouge or fractured rock was used, a memory of the maximum load experienced was

439 retained. This is evidenced by considerable hysteresis on the unloading cycle of the test history

440 (Figure 4, Figure 7, Figure 8b). The unloading response can also be seen to be described by a

441 power-law or cubic relationship. For COx, a power-law of $18.5\ \sigma_n^{-0.6}$ is observed. The situation

442 for kaolinite gouge is somewhat different. Initially there is no recovery of flow, until at a

443 threshold vertical stress the flow recovers as described by a power-law. However, a cubic

444 relationship adequately describes the full unload response. Similar hysteresis has been noted in

445 Opalinus clay (Cuss *et al.,* 2011; 2014). The unload history of three tests are shown in Figure

446 10. The data for Opalinus clay (Cuss *et al.*, 2011) were not originally reported in terms of

447 hysteresis. However, a reinterpretation of the data shows the initial testing state was to increase

448   vertical stress to a maximum value and measure flow during unloading steps. As shown, little

449   recovery of flow was experienced. Figure 10 also shows hydraulic flow data measured on

450   fractured COx within an isotropically loaded test configuration (COx_4; Harrington *et al.*,

451   2017). This dataset was also measured from a maximum stress state in lowered stress steps and

452   can be defined by a power-law relationship. The observation of such behaviour in tests

453   conducted in isotropic and shear test configurations demonstrates that the power-law unloading

454   response is not purely an artefact of the test geometry used.

455   The observation of hystersis can be explained using classical soil mechanics. The loading stage

456   of the fracture follows the virgin consolidation line (VCL) with the change in flow described

457   by a power-law relationship. Unloading follows the rebound reconsolidation line (RRL), with

458   a partial recovery of flow properties, due mainly to a recovery in void ratio in response to a

459   lowering of stress. However, in all tests described there are considerable differences seen at

460   stress levels depending on whether observed during a loading or unloading stress state. This

461   illustrates the importance of stress history on predicting flow along discontinuities and has been

462   used to explain the non-applicability of the critical stress approach in its simple form for a UK

463   site (Sathar *et al.*, 2012). Other processes, such as surface charge of clay minerals opposing

464   recovery of porosity on unloading and non-recovery of flow related to clay swelling in response

465   to increasing stress changes, may also be contributing to the observed hysteresis; these

466   processes require further investigation. Therefore, stress history is an important control on

467   fracture flow and consideration only of the current stress state may lead to inaccuracies in the

468   prediction of flow in fractured mudrocks.

469   Figure 8 shows that a power-law can describe the relationship between flow and vertical stress

470   for COx. Different slopes are noted, as are different intercepts. For instance, at 3 MPa vertical

471   stress the fracture transmissivity is 6.8×10^{-14} m^2 s^{-1} for test DSR_COx_01 compared to $1.9 \times$

472   10^{-14} m^2 s^{-1} for test DSR_COx_2. This difference can be attributed to the orientation of the test

473   samples, or may be due to the difference in durations of test stages in the two experiments. Test

474   DSR_COx_01 was orientated with a fracture parallel to the bedding, whilst test DSR_COx_02

475   was fractured perpendicular to bedding. These differences are also noted in the vertical

476   displacement (dilation/contraction of the fracture) seen during the experiment. For test

477   DSR_COx_01, a total of 0.07 mm of displacement was noted, whereas nearly 0.25 mm was

478   seen in test DSR_COx_02. This suggests that a fracture perpendicular with bedding

479   accommodates greater compression and explains why a lower fracture transmissivity is

480   observed. The swelling characteristics are also dissimilar between the tests. As stated earlier,

481   test DSR_COx_01 showed a considerable time-dependent response early in the test history,

482   suggesting that a fracture parallel to bedding exhibits greater time-dependent swelling

483   compared with a fracture oriented perpendicularly. Test DSR_COx_02 would be expected to

484   show greater swelling characteristics given a lower starting saturation of the test sample. These

485   results show that fracture orientation with respect to bedding may play a role on the flow

486   properties, both magnitude and stress sensitivity of flow. However, it has to be acknowledged

487   that the test histories of the two experiments are considerably different and the super-position

488   of mechanical and swelling responses may be the cause of these observations.

489   Comparisons can be made between the current experiments and those conducted on fractures

490   in Opalinus Clay (OPA). Cuss *et al.* (2009; 2011) describe the variation of fracture flow

491   dependence on normal stress for an idealized planed fracture in OPA. A hydraulic

492   transmissivity of approximately 5×10^{-14} m^2 s^{-1} was observed, which is comparable with the

493    $0.5 – 6 \times 10^{-14}$ m^2 s^{-1} seen in the current study for kaolinite and $0.8 – 16 \times 10^{-14}$ m^2 s^{-1} seen in

494   COx.

495   The current study has shown that hydraulic flow along fractures within the engineering

496   disturbed zone (EDZ) surrounding an underground geological disposal facility for radioactive

497   waste in Callovo-Oxfordian mudstone will have a stress-dependent response. This can be

498 defined by a cubic-law relationship for either individual fractures, as determined from

499 laboratory experiments, or for the bulk rock mass, as determined from *in situ* experiments.

500 Fracture flow reduces as the stress acting across a fracture increases. Therefore, swelling of

501 Callovo-Oxfordian mudstone or engineered sealing components will result in a reduction in

502 flow and if sufficient, this will reduce to that seen in the intact rock. This study also showed

503 that the flow along EDZ fractures will have a stress-memory and will be similar to the

504 maximum stress that has been experienced by the rock. This hysteresis means that future

505 reductions in loading of the rock will not resort in significant recovery of enhanced flow.

506 **5. Conclusions**

507 This paper describes an experimental study of four loading-unloading experiments conducted

508 on kaolinite gouge on a 30° slip-plane and shear fractures created in COx. The main

509 conclusions of the study are:

510 a. The observed response of fracture transmissivity to normal stress in COx is a complex

511   superposition of mechanical response of the fracture and the swelling of clay in the fracture

512   surface;

513 b. During a loading (vertical stress) and unloading cycle, hysteresis in flow was observed

514   signifying the importance of stress history on fracture flow. Consideration of just the

515   current stress acting upon a fracture, and not a history of stress variation, may therefore

516   result in an inaccurate prediction of hydraulic flow;

517 c. The stress dependency of fracture flow in both kaolinite and COx can be described by a

518   power-law or cubic relationship. Sufficient data are not yet available to fully understand

519   the physical controls on the parameters of the relationship observed;

520   d. During unloading stages only partial recovery of flow was observed in kaolinite and COx.

521   This partial recovery of flow has been observed in isotropically-loaded samples and shows

522   that the behaviour is not a simple artefact of the test geometry;

523   e. COx showed a considerable time-dependent behaviour, indicating that it has a good self-

524   sealing potential as clay minerals swell once they are hydrated;

525   f. Fracture orientation with respect to bedding may play a role on flow properties, both

526   magnitude and stress sensitivity of flow. A fracture parallel with bedding accommodates

527   greater compression and results in a lower transmissivity;

528   g. Observations of flow within a clay-filled gouge showed a consistent behaviour to the

529   mechanical response seen for COx, showing that the simplified experimental geometry

530   effectively replicated the flow observed in real fractures. However, the addition of swelling

531   in COx gives a more complex stress-dependent flow.

532   **Acknowledgements**

543   **References**

544 Armand, G., Leveau, F., Nussbaum, C., de La Vaissiere, R., Noiret, A., Jaeggi, D., Landrein,
545 P., and Righini, C. (2014) Geometry and properties of the excavation-induced fractures at the
546 Meuse/Haute-Marne URL drifts. *Rock Mech Rock Eng* 2014; **47**(1): pp.21–41.

547 Auvray, C., Morlot, C., Fourreau, E. and Talandier, J. (2015) X-Ray Tomography Applied to
548 Self-Healing Experiments on Argillites. In *13th ISRM International Congress of Rock
549 Mechanics*. International Society for Rock Mechanics.

550 Barla, M. (1999) Tunnels in swelling ground: Simulation of 3-D triaxial tests by triaxial
551 laboratory testing. PhD Thesis, Technical University of Turin, Italy, 179p.

552 Berkowitz, B. (2002) Characterizing flow and transport in fractured geological media: A
553 review. *Advances in water resources*, **25**(8), pp.861-884.

554 Bonini, M. Barla, M. and Barla, G. (2001) Flac applications to the analysis of swelling
555 behaviour in tunnels. 2nd Flac Symposium on Numerical Modeling in Geomechanics, Lione,
556 29-31 October, 2001

557 Bossart, P., Meier, P. M., Moeri, A., Trick, T., and Mayor, J.-C. (2002) Geological and
558 hydraulic characterisation of the excavation disturbed zone in the Opalinus Clay of the Mont
559 Terri Rock Laboratory. Engineering Geology, 66 (1-2), pp. 19-38.

560 Bossart, P., Trick, T., Meier, P.M. and Mayor, J.C. (2004) Structural and hydrogeological
561 characterisation of the excavation-disturbed zone in the Opalinus Clay (Mont Terri Project,
562 Switzerland). *Applied clay science*, **26**(1), pp.429-448.

563 Bühler, C., Heitz, D., Trick, T., and Frieg, B. (2003) In-Situ Self-Sealing of the EDZ as a
564 Consequence of Loading. In: Davies, C and Bernier, F. (Eds.) Impact of the Excavation
565 Disturbed or Damaged Zone (EDZ) on the Performance of Radioactive Waste Geological
566 Repositories. Proceedings of a European Commission CLUSTER Conference and Workshop
567 Luxembourg, 3 to 5 November 2003. EUR 21028 EN pp.281-286.

568 Cuss, R.J. and Harrington, J.F. (2014) Experimental observations of the flow of water and gas
569 along fractures in Opalinus Clay. Extended abstract We07. Fourth EAGE Shale Workshop,
570 6-9 April 2014, Porto, Portugal.

571 Cuss, R.J., Graham, C.C., Wiseall, A.C, and Harrington, J.F. (2016) Cyclic loading of an
572 idealized clay-filled fault; comparing hydraulic flow in two clay gouges. *Geofluids*, **16**,
573 pp.552-564. DOI: 10.1111/gfl.12175.

574 Cuss, R.J., Harrington, J.F., Milodowski, A.E., and Wiseall, A.C. (2014). Experimental study
575 of gas flow along an induced fracture in Opalinus Clay. British Geological Survey
576 Commissioned Report, CR/14/051. 79pp.

577 Cuss, R.J., Milodowski, A., and Harrington, J.F. (2011) Fracture transmissivity as a function
578 of normal and shear stress: first results in Opalinus clay. Physics and Chemistry of the Earth.
579 36, pp. 1960-1971.

580 Cuss, R.J., Milodowski, A.E., Harrington, J.F. and Noy, D.J. (2009) Fracture transmissivity
581 test of an idealised fracture in Opalinus Clay. British Geological Survey Commissioned
582 Report, CR/09/163. 74pp.

583 Cuss, R.J., Sathar, S., and Harrington, J.F. (2012) Fracture transmissivity test in Opalinus Clay;
584 test conducted on a realistic fracture. British Geological Survey Commissioned Report,
585 CR/12/132. 52pp.

586 Cuss, R.J., Sathar, S., and Harrington, J.F. (2013) Final Report of FORGE WP4.1.2: Validation
587 of critical stress theory applied to repository concepts. British Geological Survey
588 Commissioned Report, CR/13/001. 96pp.

589 David, C., Wong, T.F., Zhu, W., and Zhang, J. (1994) Laboratory measurement of compaction-
590 induced permeability change in porous rocks; implications for the generation and

591   maintenance of pore pressure excess in the crust. Pure and Applied Geophysics, 143, pp. 425-
592   456.

593   Davy, C.A., Skoczylas, F., Barnichon, J.D. and Lebon, P. (2007) Permeability of macro-
594   cracked argillite under confinement: gas and water testing. *Physics and Chemistry of the*
595   *Earth*, Parts A/B/C, **32**(8), pp.667-680.

596   de La Vaissière, R., Armand, G., and Talandier, J. (2015) Gas and water flow in an excavation-
597   induced fracture network around an underground drift: A case study for a radioactive waste
598   repository in clay rock. *Journal of Hydrology*, **521**, pp.141-156.
599   doi:10.1016/j.jhydrol.2014.11.067

600   Dewhurst, D.N., Aplin, A.C., and Sarda, J.-P. (1999[1]) Influence of clay fraction on pore-scale
601   properties and hydraulic conductivity of experimentally compacted mudstones. Journal of
602   Geophysical Research, 104, pp. 29,261-29,274.

603   Dewhurst, D.N., Aplin, A.C., Sarda, J.-P., and Yang, Y. (1998) Compaction-driven evolution
604   of porosity and permeability in natural mudstones: An experimental study. Journal of
605   Geophysical Research, 103, pp. 651-661.

606   Dewhurst, D.N., Yang, Y., and Aplin, A.C. (1999[2]) Permeability and fluid flow in natural
607   mudstones. In: Aplin, A.C., Fleet, A.J., and Macquaker, J.H.S., eds., Mud and Mudstones:
608   Physical and Fluid Flow Properties, Geological Society of London, Special Publications, 158,
609   pp. 23-43.

610   Foct, F., Semete, P., Desgree, P., Imbert, C. and Talandier, J. (2012) Hydraulic sealing of
611   fractured argillaceous rocks. *Clays in Natural and Engineered Barriers for Radioactive Waste*
612   *Confinement*. 5th International Meeting. Montpellier, October 22nd – 25th, 2012.

613   Gaucher, E.C., Lerouge, C., Blanc, P., and Tournassat, C. (2007) Caractérisation géochimique
614   des forages PAC et nouvelles modélisations THERMOAR. *BRGM*. **RP-54416-FR**.

615   Gutierrez, M., Øino, L.E. and Nygard, R. (2000) Stress-dependent permeability of a de-
616   mineralised fracture in shale. Marine and Petroleum Geology, 17, pp.895–907.

617   Harrington, J.F., Cuss, R.C. and Talandier, J. (2017) Gas transport properties through intact
618   and fractured Callovo-Oxfordian mudstones. In: Rutter, E.H., Mecklenburgh, J. & Taylor,
619   K.G. (eds) *Geomechanical and Petrophysical Properties of Mudrocks*. Geological Society,
620   London, Special Publications, **454**. https://doi.org/10.1144/SP454.7

621   Holt, RM (1990) Permeability reduction induced by a non-hydrostatic stress field. SPE
622   Formation Evaluation, Dec 1990, pp. 444–448.

623   Katsube, T.J. (2000) Shale permeability and pore-structure evolution characteristics.
624   Geological Survey of Canada. Ottawa, ON, Canada. Pages: 9.

625   Katsube, T.J., Boitnott, G.N., Lindsay, P.J., and Williamson, M. (1996) Pore structure
626   evolution of compacting muds from the seafloor, offshore Nova Scotia. In: Anonymous, ed.,
627   Eastern Canada and national and general programs. Current Research - Geological Survey of
628   Canada, pp. 17-26.

629   Katsube, T.J., Issler, D.R., and Coyner, K. (1996) Petrophysical characteristics of shale from
630   the Beaufort-Mackenzie Basin, northern Canada; permeability, formation factor, and porosity
631   versus pressure, Interior plains and Arctic Canada. Current Research - Geological Survey of
632   Canada. pp. 45-50.

633   Katsube, T.J., Mudford, B.S., and Best, M.E. (1991) Petrophysical characteristics of shales
634   from the Scotian shelf. Geophysics, 56, pp.1681-1689.

635   Keaney, G.M.J., Meredith, P.G., and Murrell, S.A.F. (1998) Laboratory study of permeability
636   evolution in a 'tight' sandstone under non-hydrostatic stress conditions. Rock Mechanics in

Petroleum Engineering, 1 8-10 July 1998, Trondheim, Norway, Society of Petroleum Engineers, SPE/ISRM 47265, pp. 329-335.

Kwon, O., Kronenberg, A.K., Gangi, A.F., and Johnson, B. (2001) Permeability of Wilcox Shale and its effective pressure law. Journal of Geophysical Research, B, Solid Earth and Planets, 106, pp. 19,339-19,353.

Morrow, C., Shi, L.Q., and Byerlee, J.D. (1984) Permeability of fault gouge under confining pressure and shear stress. Journal of Geophysics Research, 89, pp. 3193-3200.

Neuzil, C.E., Bredehoeft, J.D. and Wolff, R.G. (1984) Leakage and fracture permeability in the Cretaceous shales confining the Dakota aquifer in South Dakota. In: Proceedings of First C.V. Theis Conference on Geohydrology in Dublin, Ohio. Jorgensen, D.G. and Signor, D.C. (eds.). National Water Well Association. pp.113-120.

Rutqvist, J., Börgesson, L., Chijimatsu, M., Hernelind, J., Jing, L., Kobayashi, A., and Nguyen, S. (2009) Modeling of damage, permeability changes and pressure responses during excavation of the TSX tunnel in granitic rock at URL, Canada. Environmental Geology, 57 (6), pp. 1263-1274.

Sathar, S., Reeves, H.J., Cuss, R.J., and Harrington, H.J. (2012) Critical stress theory applied to repository concepts; the importance of stress tensor and stress history in fracture flow. Mineralogical Magazine. December 2012, 76 (8), pp. 3165-3177.

Schloemer, S., and Krooss, B.M. (1997) Experimental characterisation of the hydrocarbon sealing efficiency of cap rocks. Marine and Petroleum Geology, 14, pp. 565-580.

Walsh, J.B., and Brace, W.F. (1984) The effect of pressure on porosity and the transport properties of rock. Journal of Geophysical Research. B, 89, pp. 9425-9431.

Yven, B., Sammartino, S., Géraud, Y., Homand, F., and Villiéras, F. (2007) Mineralogy, texture and porosity of Callovo-Oxfordian argillites of the Meuse/Haute-Marne region (eastern Paris Basin). *Mémoires de la Société géologique de France*, **178**, pp.73–90.

Zhang, C.-l., Czaikowski, O., Rothfuchs, T., and Wieczorek, K. (2013) Thermo-Hydro-Mechanical Processes in the Nearfield around a HLW Repository in Argillaceous Formations; Volume I: Laboratory Investigations May 2007 to May 2013. *GRS report*, **GRS-312**, 342pp., ISBN 978-3-939355-91-5

Zhang, C. and Rothfuchs, T. (2004) Experimental study of the hydro-mechanical behaviour of the Callovo-Oxfordian argillite. Applied Clay Science, 26(1), pp.325-336.

Zhu, W., and Wong, T.f. (1994) Permeability evolution related to the brittle-ductile transition in Berea Sandstone. In: Anonymous, ed., AGU 1994 fall meeting., 75; 44 Suppl.: Eos, Transactions, American Geophysical Union. pp. 638.

Zhu, W., and Wong, T.-f. (1997) The transition from brittle faulting to cataclastic flow; permeability evolution. Journal of Geophysical Research, B, Solid Earth and Planets, 102, pp. 3027-3041.

Zoback, M.D., and Byerlee, J.D. (1975) The effect of microcrack dilatancy on the permeability of Westerly Granite. Journal of Geophysics Research, 80, pp. 752-755.

676   a.
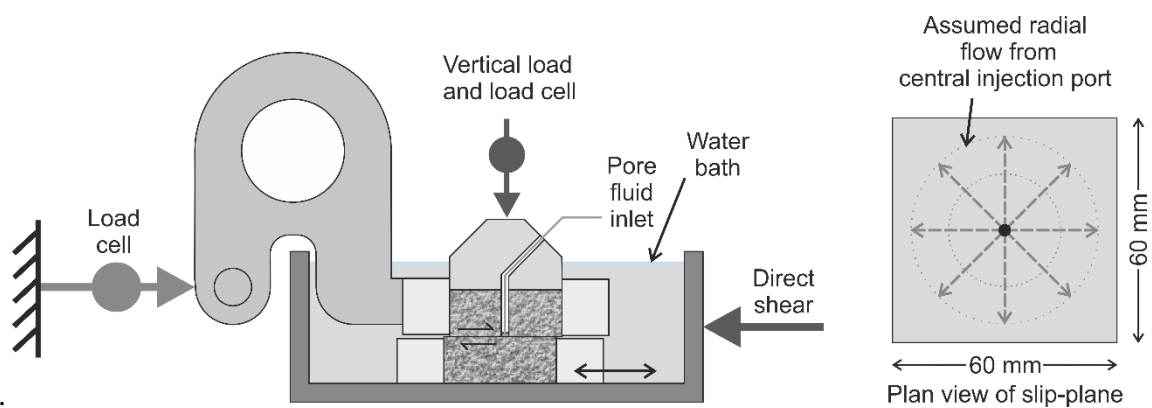
677   b.
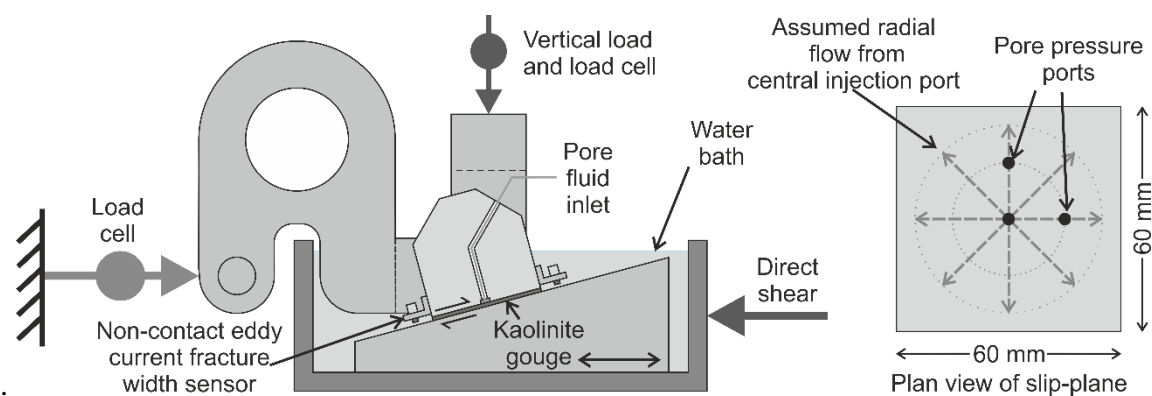
678   **Figure 1**   Schematic of the (a) Direct Shear Rig and (b) Angled Shear Rig experimental
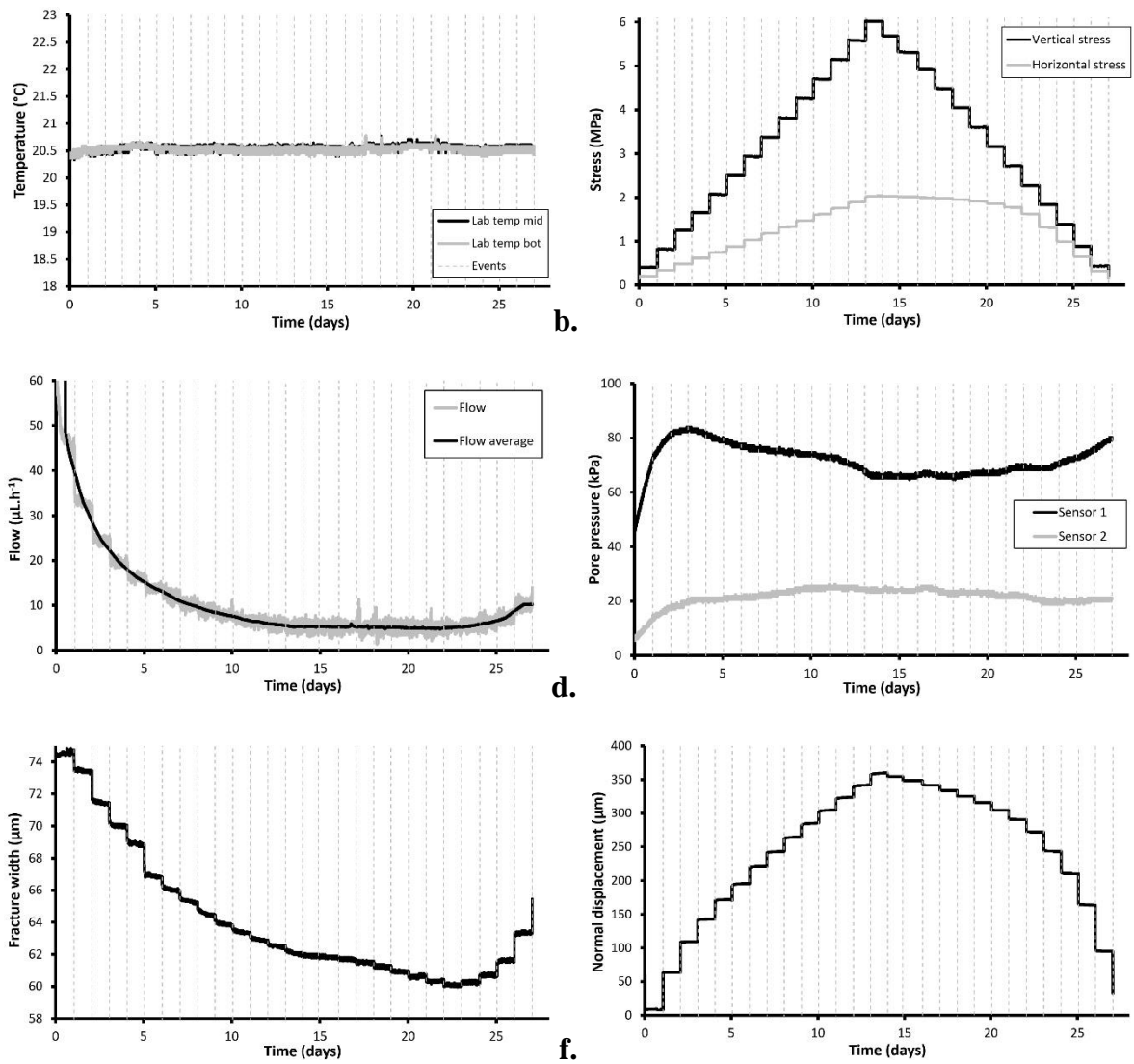
679   apparatus.

680 **a.**
681 **c.**
682 **e.**

683 **Figure 2** Example results from a hydraulic test conducted on a kaolinite gouge plotted against

684 time (ASR_Tau05_30wLU): a) Temperature; b) Vertical and horizontal stress; c) Hydraulic

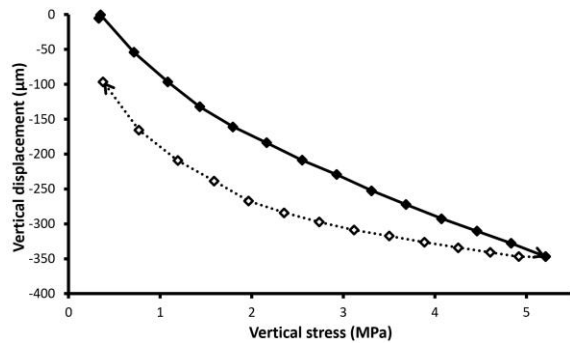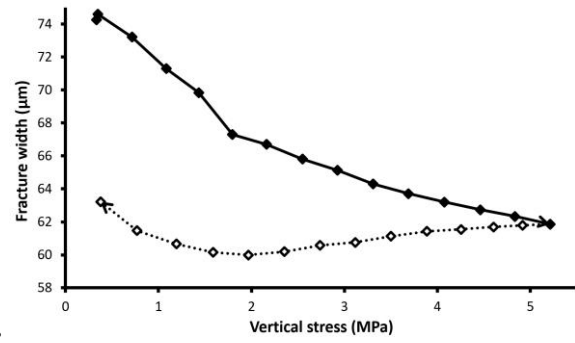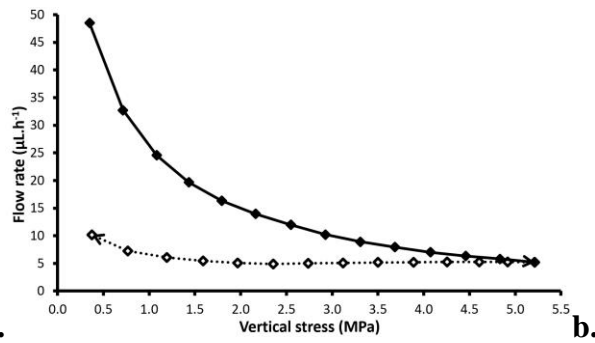685 flow; d) Pore pressures within the slip plane; e) Fracture width; f) Normal displacement.

686   **a.**

687   **c.**

688   **Figure 3** Example results from a hydraulic test conducted on a kaolinite gouge plotted against

689   vertical stress (ASR_Tau05_30wLU): a) Hydraulic flow; b) Fracture width; c) Normal

690   displacement.

691
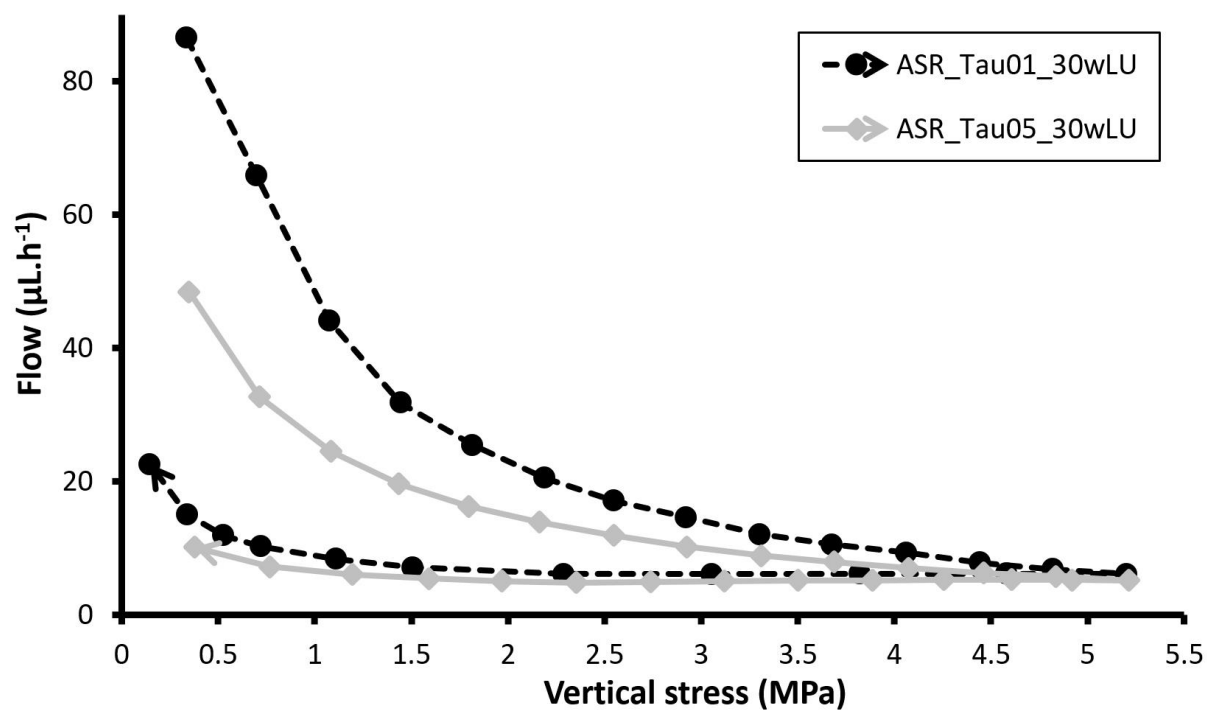
Figure 4 Comparison of two tests conducted on kaolinite gouge showing hysteresis in hydraulic flow during loading/unloading experiments on a 30° slip-plane.
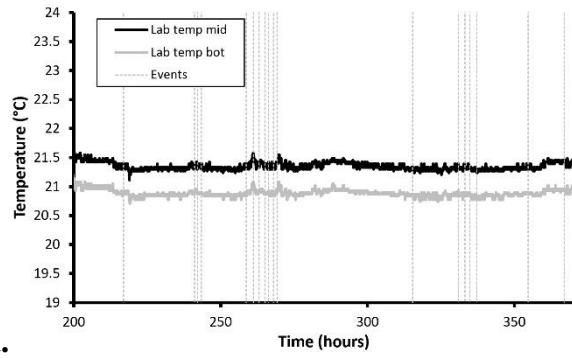
694 **a.**

695 **c.**

696 **e.**

697 **g.**
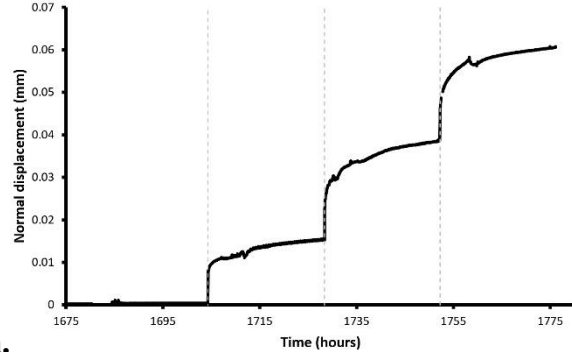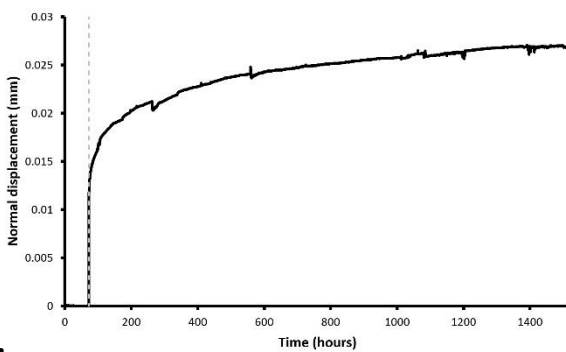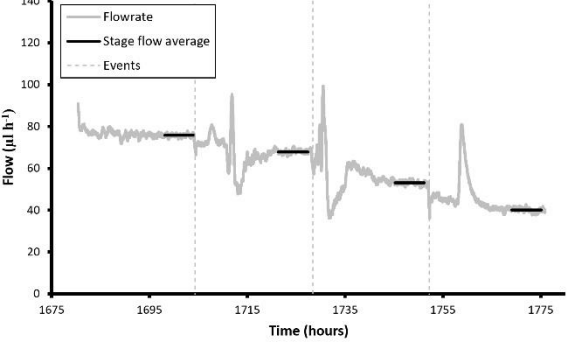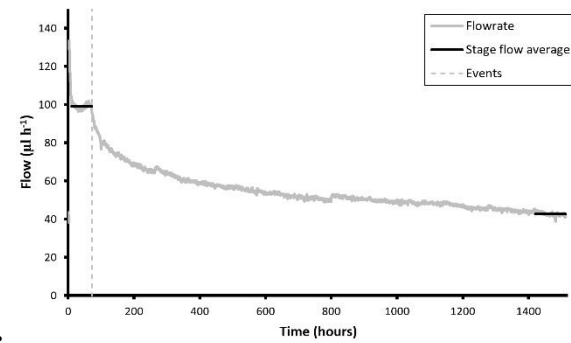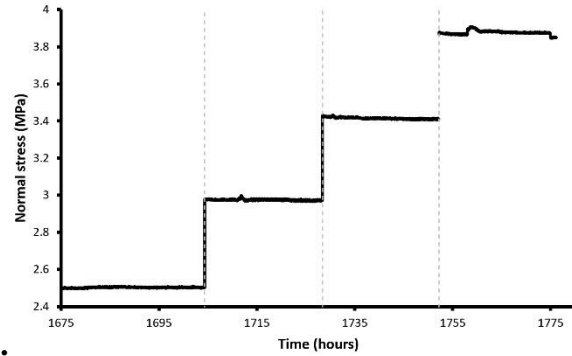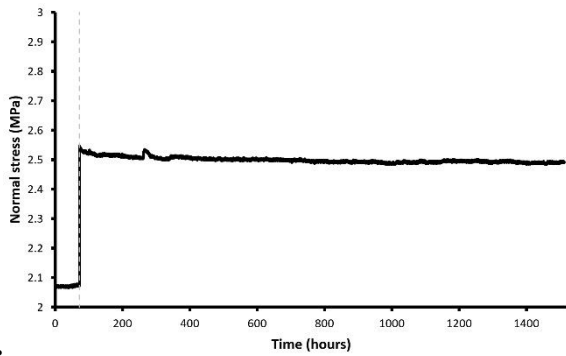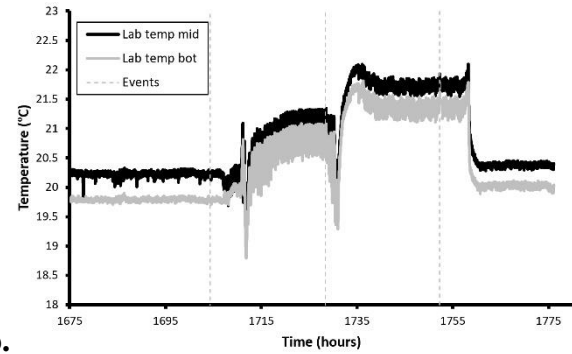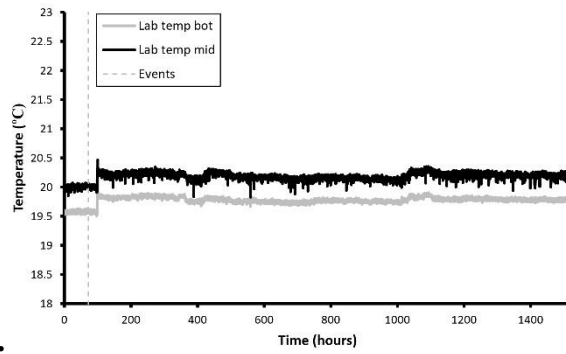
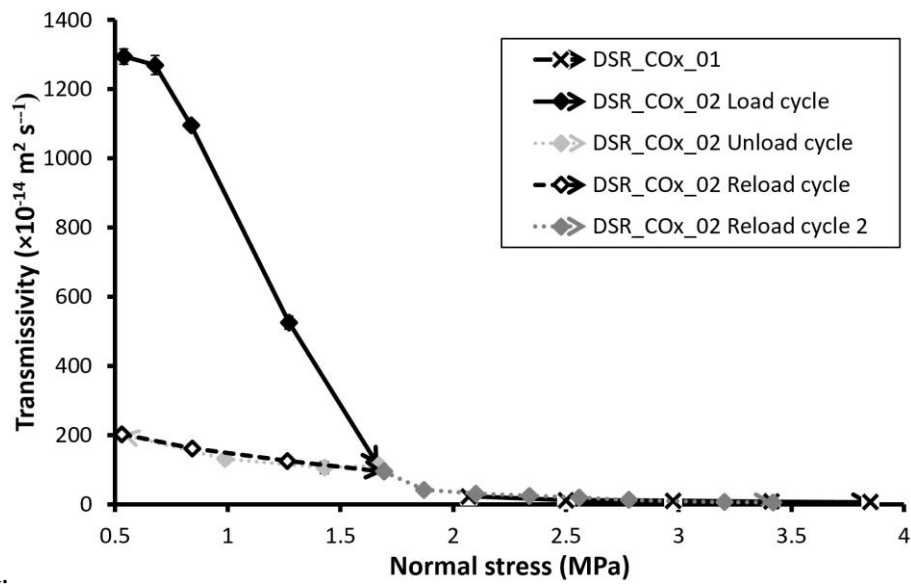698 **Figure 5** Results from hydraulic test DSR_COx_01 conducted on COx plotted against time: a-

699 b) Temperature; c-d) Normal stress; e-f) Hydraulic flow; g-h) Normal displacement. Figure a,

700 c, e and f represent stage 1 of the test, whilst b, d, f, h represent stage 2.

701 **a.**

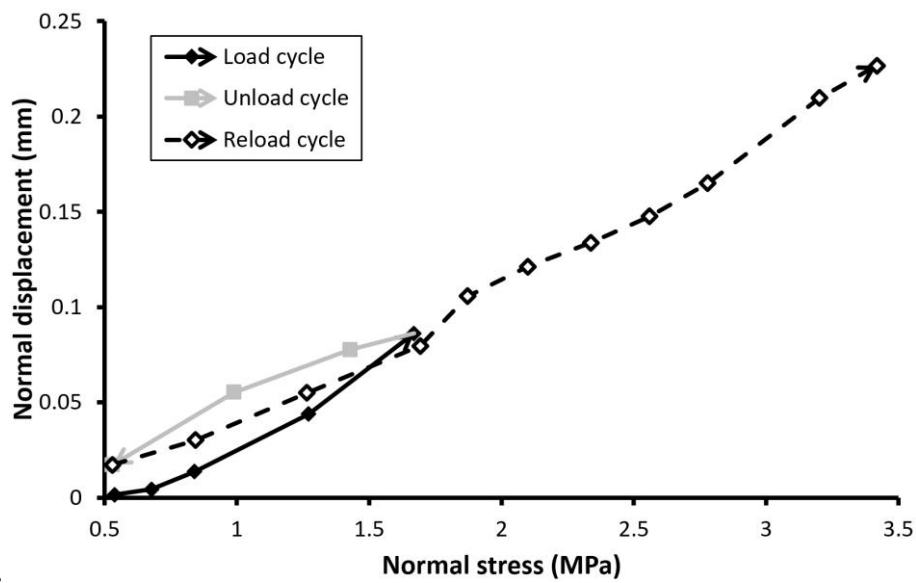702 **c.**

b.

d.
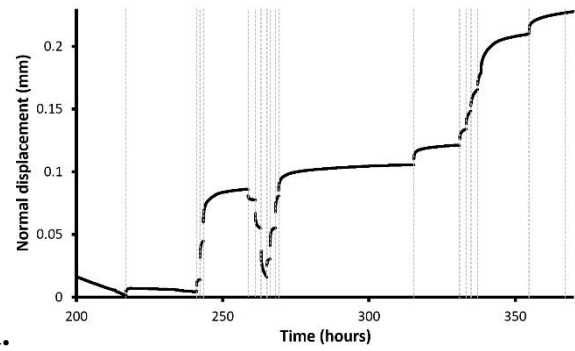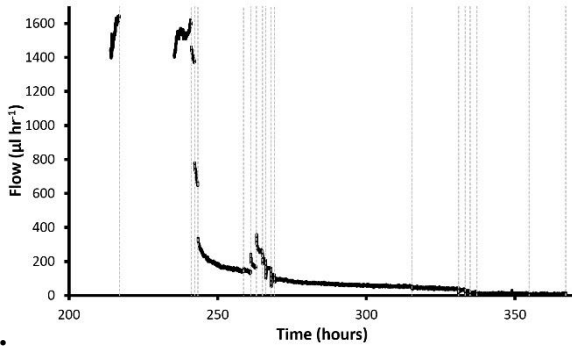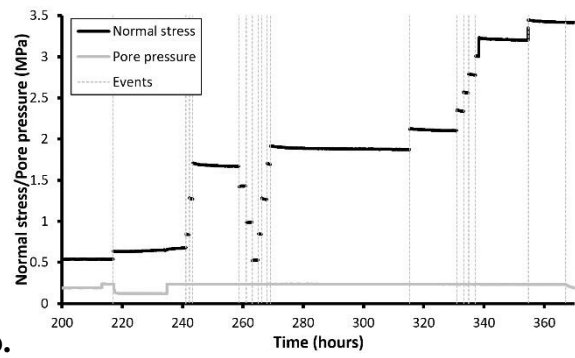
703 **Figure 6** Results from hydraulic test DSR_COx_02 conducted on COx plotted against time: a)

704 Temperature; b) Normal stress and pore pressure; c) Hydraulic flow; d) Normal displacement.

705

706

707   a.

708   **b.**

709   **Figure 7** Results from two hydraulic tests conducted on fractured COx against vertical stress:

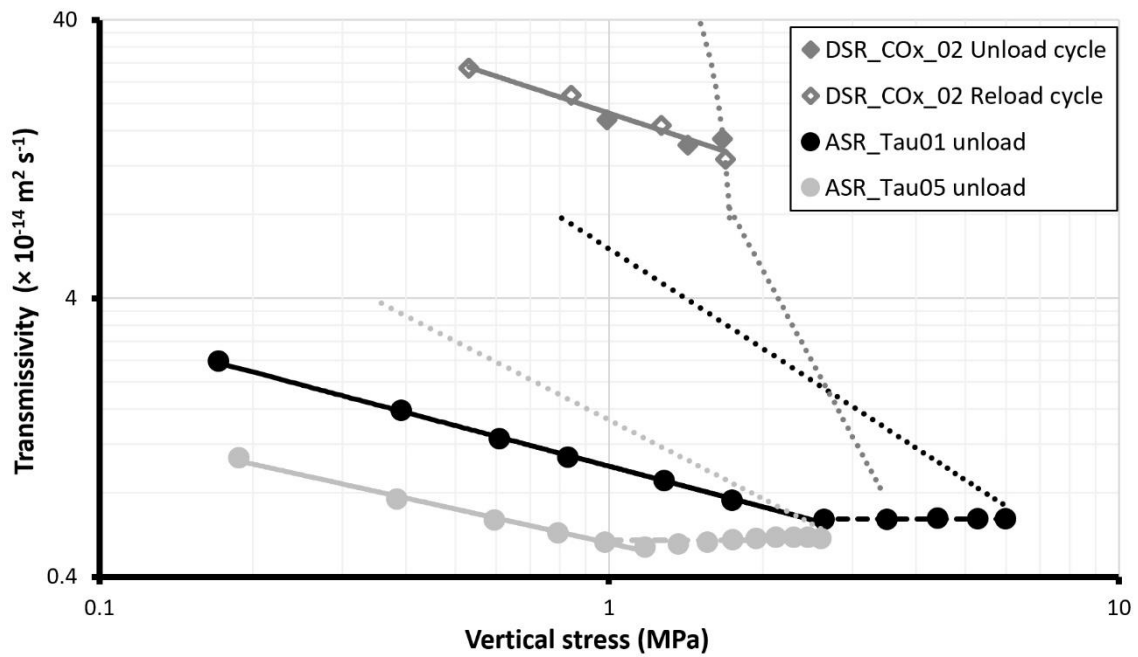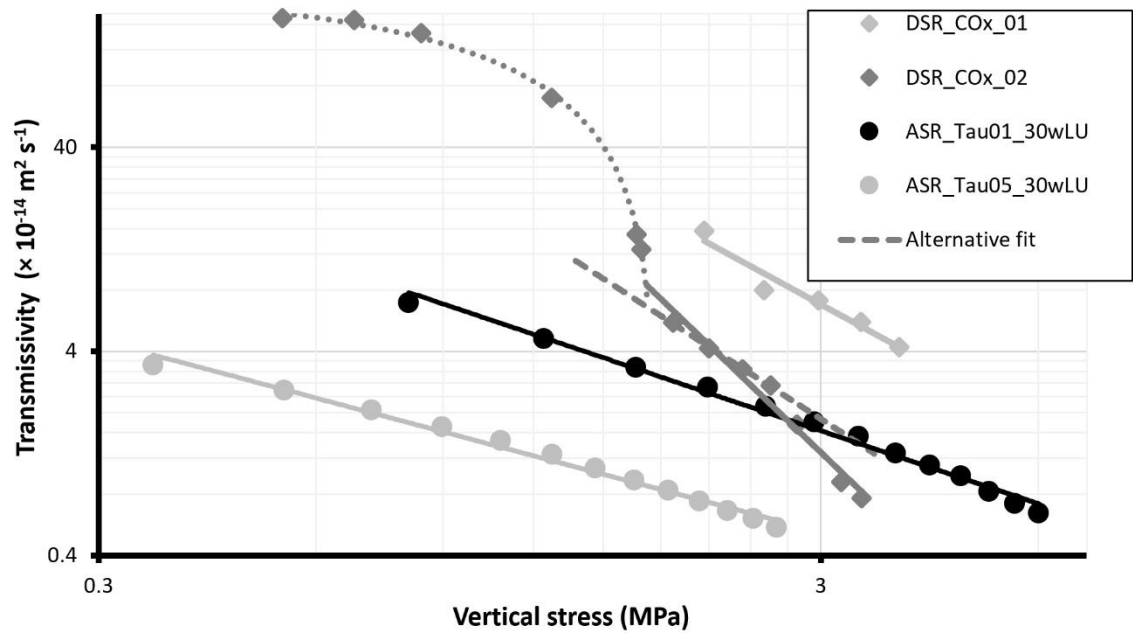710   a) Hydraulic flow; b) Normal displacement (Note: test DSR_COx_02 only).

711 **a.**

712 **b.**

713 **Figure 8** Results for relationship of fracture transmissivity with vertical stress in fractured

714 COx: a) loading response; b) unloading.
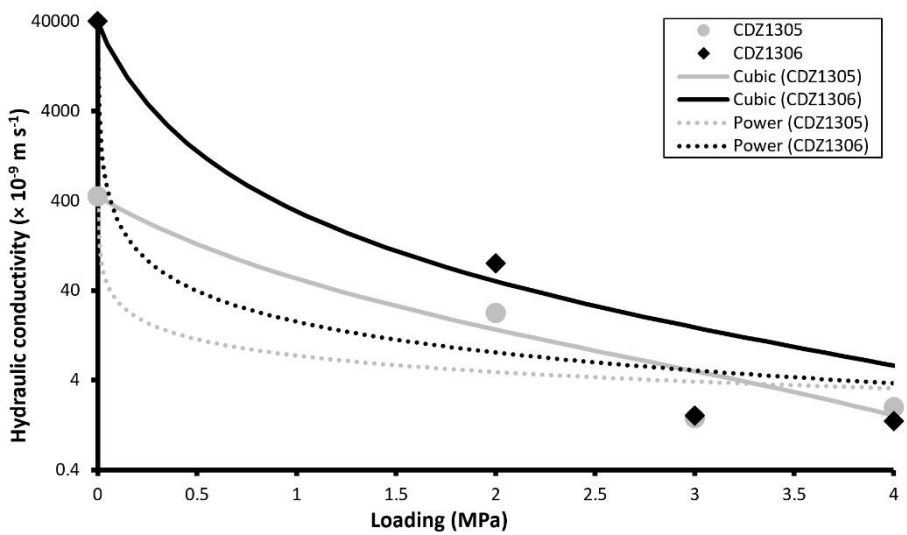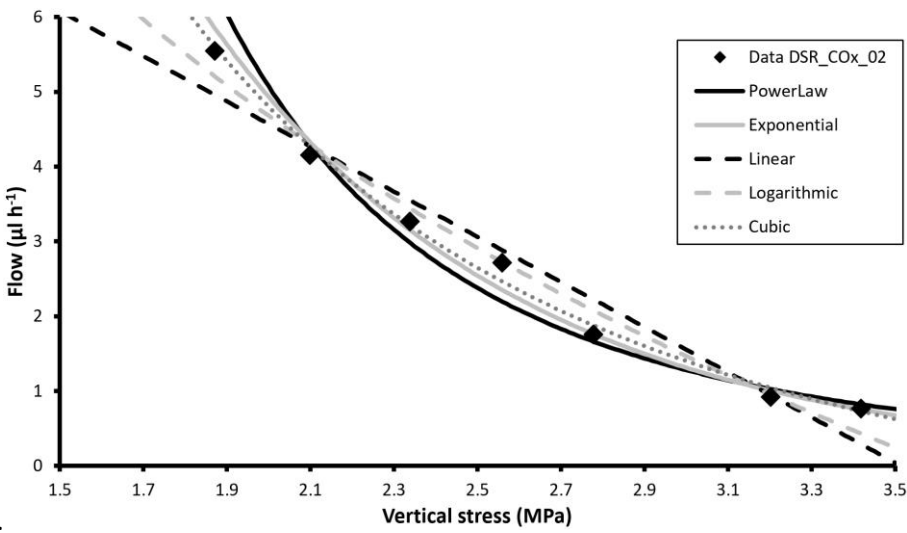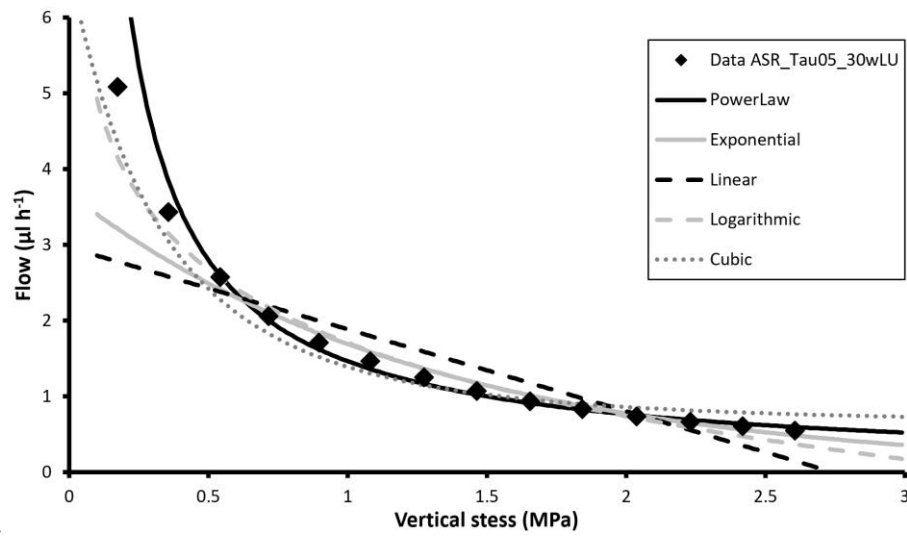
715

716   a.

717   b.

718   c.

719   **Figure 9** Comparing five best-fit relationships to the experimental data; a) test ASR_Tau05,

720   b) DSR_COx_02. The power-law fit is seen to best describe the data, especially at the initial

721　loading stage at low vertical stress, c) Cubic-law fit to test data from the in situ Compression

722　of the Damage Zone (CDZ) test conducted at the Meuse/Haute-Marne URL (de La Vaissière
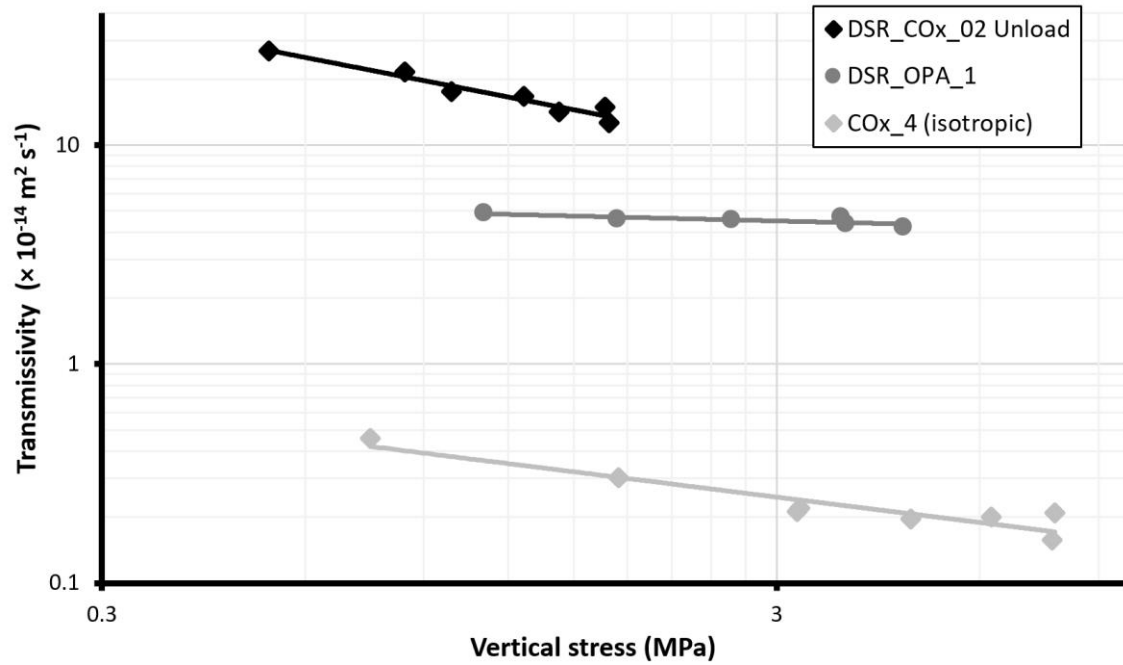
723　et al., 2015).

724

725　**Figure 10** Flow history observed during unload testing of fractures in COx and Opalinus Clay.

	DSR_COx_01	DSR_COx_02
Borehole	OHZ1607	OHZ1607
Sample number	EST44339	EST44342
Borehole depth	8.37 – 8.67 m	9.08 – 9.38 m
Date drilled	21/10/11	21/10/11
Drilling direction	Horizontal	Horizontal
Sample preparation	5/11/13	10/11/14
Sample orientation with respect to bedding	Perpendicular	Parallel
Sample dimensions (mm)	59.9 × 60.1 × 54.3	60.0 × 59.9 × 50.2
Weight (g)	470.6	426.1
Volume (cc)	195.5	181.1
Density (g/cc)	2.43	2.37
Porosity (%)	14.9	17.7
Saturation	0.935	0.80

726   **Table 1** Properties of core and sample material for shear tests conducted on COx.

Experiment	Start date	Sample Material	Water saturation (%)	Fault orientation
ASR_Tau01_30wLU	09-Nov-10	Kaolinite	98	30°
ASR_Tau05_30wLU	27-May-11	Kaolinite	98	30°
DSR_COx_01	6-Nov-13	COx	93.5	0°
DSR_COx_02	10-Nov-14	COx	92.0	0°

727 **Table 2** List of experiments described in the current study. ASR = Angled Shear Rig; DSR =

728 Direct Shear Rig; w = hydraulic test; LU = Load-unload experiment; COx = Callovo-Oxfordian

729 mudstone.

Experiment	Loading	Unloading
ASR_Tau01_30wLU	$6.0\,\sigma_n^{-1.2}$	$1.0\,\sigma_n^{-0.5}$
ASR_Tau05_30wLU	$1.5\,\sigma_n^{-1.0}$	$0.5\,\sigma_n^{-0.4}$
DSR_COx_01	$56\,\sigma_n^{-1.9}$	-
DSR_COx_02	$53\,\sigma_n^{-3.4}$	$18.5\,\sigma_n^{-0.6}$
DSR_COx_02 (alternative)	$23\,\sigma_n^{-2.3}$	-

730 **Table 3** Power-law relationships derived for loading and unloading sections of the

731 experimental data. Note: fit to flow ($\mu l\ h^{-1}$) data.

Experiment		Power-law	Exponential	Logarithmic	Linear	Cubic
ASR_Tau01_30wLU	L	**0.99**	0.97	0.94	0.76	**0.99**
	U	0.94	0.63	0.86	0.50	**0.99**
ASR_Tau05_30wLU	L	**0.99**	0.97	0.98	0.83	**0.99**
	U	0.73	0.41	0.71	0.39	**0.98**
DSR_COx_01	L	0.94	0.92	0.86	0.80	**0.95**
DSR_COx_02	L	0.86	0.94	0.96	**0.99**	
	L	0.97	**0.99**	0.98	0.95	0.91
	U	0.94	0.91	0.95	0.89	**0.99**
Average		0.92	0.84	0.90	0.77	**0.97**
Average load	L	**0.97**	0.96	0.94	0.84	0.96
Average unload	U	0.87	0.65	0.84	0.59	**0.99**

732 **Table 4** Comparison of R^2 values for best-fit relationships for loading (L) and unloading (U)

733 sections of the experimental data.